Interaction of two axisymmetric turbulent wakes

Martin Obligado, Simon Klein, J.C. Vassilicos

Interaction of two axisymmetric turbulent wakes

M. Obligado[1], S. Klein[2] and J.C. Vassilicos[3]
[1] *Université Grenoble Alpes, CNRS, Grenoble-INP, LEGI, F-38000, Grenoble, France*
[2] *Institute of Fluid Mechanics, TU Braunschweig, Braunschweig, Germany and*
[3] *Univ. Lille, CNRS, ONERA, Arts et Métiers ParisTech, Centrale Lille, UMR 9014 - LMFL - Laboratoire de Mécanique des fluides de Lille - Kampé de Feriet, F-59000 Lille, France*

The interaction between turbulent axisymmetric wakes plays an important role in many industrial applications, notably in the modelling of wind farms. While the non-equilibrium high Reynolds number scalings present in the wake of axisymmetric plates has been shown to modify the averaged streamwise scalings of individual wakes, little attention has been paid to their consequences in terms of wake interactions. We propose an experimental setup that tests the presence of non-equilibrium turbulence using the streamwise variation of velocity fluctuations between two bluff bodies facing a laminar flow. We have studied two different sets of plates (one with regular and another with irregular peripheries) with hot-wire anemometry in a wind tunnel. We first show that the wake interaction length, that quantifies the streamwise position where the wakes start interacting, can be deduced from the streamwise profiles of turbulence intensity, a quantity that is easy to resolve even in challenging field measurements. By acquiring streamwise profiles for different plate separations and identifying the wake interaction length for each separation it is therefore possible to study the interaction between two axisymmetric turbulent wakes in terms of its energy cascade and, in this case, to show that the interaction between them is consistent with non-equilibrium scalings. This work also generalises previous studies concerned with the interaction of plane wakes to include axisymmetric wakes. We find that a simple mathematical expression for the wake interaction length based on non-equilibrium turbulence scalings can be used to collapse the streamwise developments of the second, third and fourth moments of the streamwise fluctuating velocity.

I. INTRODUCTION

Recently, flow regions with non-equilibrium high Reynolds number turbulence at odds with usual Richardson-Kolmogorov phenomenology have been discovered in a number of turbulent flows [1–4], in particular axisymmetric and self-preserving turbulent wakes generated by plates with and without irregular edges. These regions are characterised by streamwise evolutions of the mean flow profiles which have only recently been documented and partially understood in experiments [5, 6]. The presence of a different set of scalings has many consequences, such as variations in the turbulent entrainment in free-shear flows [7–11] and on eddy viscosity models [12], among others. Furthermore, these regions can extend as far as about 100 plate characteristic lengths (defined as $\sqrt{\mathcal{A}}$, with $\mathcal{A}$ the frontal area of the regular/irregular plate) in the streamwise direction. A further study [13] critically revised the classical theory of high Reynolds number axisymmetric turbulent wakes [14, 15] to encompass these new scalings. Both direct numerical simulations and experiments were found to agree with the theory.

In this work we focus on the interaction of turbulent axisymmetric wakes generated by two bluff bodies. This is an important configuration, present for instance in arrays of wind or marine tidal turbines, and the interaction of the two wakes can be expected to involve non-equilibrium turbulence. While some experiments in wind tunnel controlled conditions have been performed recently [16–18], no attention has been paid to the relation between the energy cascade of the turbulent flow and the wake interaction length (defined as the streamwise distance at which two wakes merge).

The non-equilibrium predictions and the classical predictions rely on axisymmetry of turbulence wake statistics, self-preservation of $(U_\infty - \langle U \rangle)/u_0$ (with U_∞ the freestream velocity, $\langle U \rangle$ the streamwise mean velocity and $u_0 = U_\infty - U_0$ the centreline velocity deficit), turbulent kinetic energy K, turbulence dissipation ε and the sum of production and turbulent transport, and on a scaling law for the centreline turbulence dissipation [9, 13, 19]. Both sets of predictions are obtained from the Reynolds averaged streamwise momentum and turbulent kinetic energy equations leading to a closed set of equations for $u_0(x)$ and the wake half width $\delta(x)$. The equilibrium predictions for axisymmetric turbulent wakes [see 14, 15] for the streamwise evolution (along x) of u_0 and δ are

$$u_0(x) = AU_\infty \left((x - x_0)/\theta\right)^{-2/3}, \tag{1}$$

$$\delta(x) = B\theta \left((x - x_0)/\theta\right)^{1/3}, \tag{2}$$

where A and B are dimensionless constants, θ the momentum thickness and x_0 a virtual origin. For an axisymmetric wake, the momentum thickness θ is defined by

$$\theta^2 = \frac{1}{U_\infty^2}\int_0^\infty U_\infty \left(U_\infty - \langle U\rangle\right) r dr, \tag{3}$$

which is constant with x, and the wake's width is here characterised by the integral wake's half width defined by

$$\delta^2(x) = \frac{1}{u_0}\int_0^\infty \left(U_\infty - \langle U\rangle\right) r dr. \tag{4}$$

On the other hand, the non-equilibrium predictions for the streamwise evolution u_0 and δ are

$$u_0(x) = AU_\infty \left((x - x_0)/\theta\right)^{-1}, \tag{5}$$

$$\delta(x) = B\theta \left((x - x_0)/\theta\right)^{1/2}. \tag{6}$$

The only difference between equilibrium and non equilibrium scalings is in the scaling of the centreline value of ε [1], that will be different according to the nature of the energy cascade. It is then possible to model the interaction between wakes via the streamwise scaling of δ. It is expected that within the equilibrium cascade, the wake interaction length x^*, defined by $2\delta(x^*) \propto S$ (see [20, 21]), will evolve as S^3, with S the separation between the centre of the plates. Accordingly, the presence of non-equilibrium energy cascade implies that $x^* \propto S^2$.

We present experimental evidence that the non-equilibrium theory in [13] properly models the interaction of two axisymmetric wakes, for plates with both regular and irregular edges. We show that, by having knowledge of the values of the wake width δ and the centreline velocity deficit u_0 for a single wake, it is possible to predict the length x^* which quantifies the position where the wakes meet. Furthermore, it is also possible to predict the intensity of the fluctuations at that particular point. For this purpose, we propose an experimental setup where streamwise profiles of streamwise fluctuating velocities are acquired via hot-wire anemometry in a wind tunnel. We introduce a method where the interaction of wakes can be characterised using the streamwise evolution of the turbulence intensity between both plates. To that aim, we have tested two different sets of plates, one with square regular and another with irregular edges.

The possibility of modelling the interaction of wakes using the properties of an isolated one is widely used in wind energy modelling. For instance, it is at the core of superposition methods [22, 23], used to model wind farms. Such applications usually rely on field data that is unresolved in the small temporal/spatial scales (such as Lidar scans [24, 25]). The method discussed here to quantify the wake interaction length, that rely only only on the rms and averaged values of the streamwise velocity, is therefore compatible with such experimental techniques and conditions.

This work generalizes previous studies on the interaction of plane wakes (see [21]) to include axisymmetric wakes. We find that the derivation of the wake interaction length proposed in this cited work can be used to collapse the streamwise development of the first three fluctuating velocity moments. Our results suggests that non-equilibrium scalings are in good agreement with the interaction of wakes for both sets of plates studied.

II. EXPERIMENTAL SETUP

The experiments were conducted in a low turbulence wind tunnel with a test-section of 3×3 ft^2 (0.91×0.91 m^2) and 4.25 m long. The bluff plates were placed at the beginning of the test-section. Figure 1a presents a sketch of the wind tunnel setup. Two solid iron bars (with a diameter of 16 mm) fixed to the wind tunnel sidewalls close to ceiling and bottom served as main support for the plates. Each plate was fixed to a thin iron rod (diameter 1.5 mm, length 750 mm) using two (vertically aligned) screws. Within this configuration, no vibrations were observed in the plates. The thin iron rods were connected to the main support by two pairs of T-like casings. These casings were attached movably to the main support bars to allow changes in plate separation. By means of small grub screws, the T-casings could be fixed to the main support bars.

We tested two different sets of plates (each set composed of two plates): one set with regular square peripheries and other set with irregular peripheries. These irregular plates, shown in figure 1b, are identical to those used in some previous works [5, 6, 13]. The perimeter shape of this plate results from a geometric self-similar process leading, if continued *ad infinitum*, to a plate with fractal perimeter of infinite length and fractal dimension $D_f = 1.5$ but the same surface area $\mathcal{A}$. The irregular plate used here corresponds to the second iteration, that has been found to produce larger values of drag coefficient and velocity deficits than other plates with both regular and irregular peripheries [5]. The regular plate has been chosen to have square peripheries, and therefore constitutes a canonical

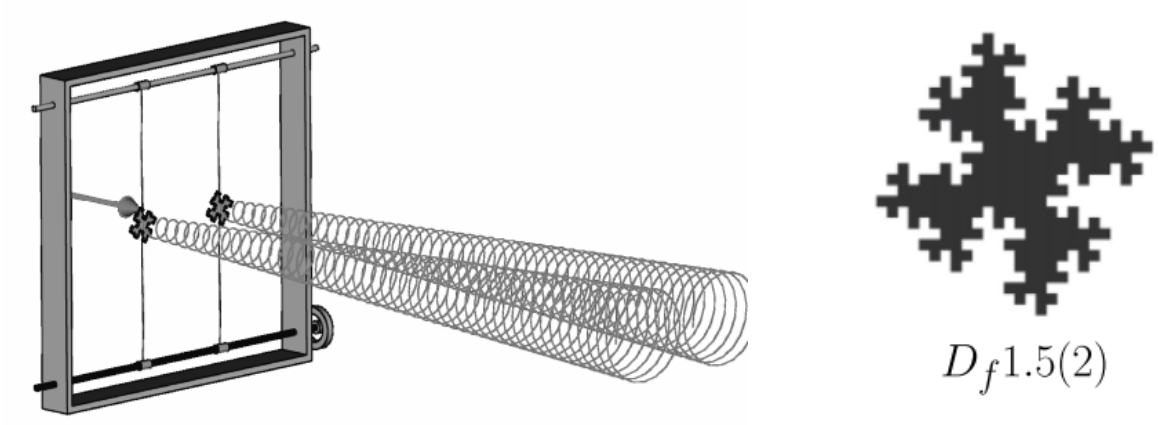

(a) (b)

FIG. 1. (a) Sketch of the experimental wind tunnel setup; (b) Irregular plate used herein. They are the second iteration of a fractal plate with dimension $D_f = 1.5$ and a square initial pattern, as characterised by [26].

configuration that will be compared to the other plates. We remark that non-equilibrium scalings have been found on a single axisymmetric wake generated by both types of plates studied here (square/regular and irregular [6, 13]). Furthermore, such scalings have been reported on the same streamwise range covered in this study ($10 < x/\sqrt{\mathcal{A}} < 50$). The main difference in the evolution of the single wake of regular and irregular plates is then due to the larger values of velocity deficit and local Reynolds number generated by the latter (defined as $Re_L = u'\sqrt{\mathcal{A}}/\nu$, with u' the standard deviation of the streamwise fluctuating velocity $u(t)$ and ν the kinematic viscosity of the fluid).

All plates studied have a reference length of $L_b = \sqrt{\mathcal{A}} = 64$ mm (with $\mathcal{A}$ the frontal area of the plates) and a thickness of 1.25 mm. Only interactions of the turbulent wakes of the same type of plate were studied, therefore we did measurements with two regular and two irregular plates only. The plates were located vertically in the symmetry plane of the wind tunnel, normal to the laminar freestream velocity. In the spanwise direction, they were equally spaced to the streamwise symmetry plane. The total blockage of the setup remains low, close to 4.3%, and therefore we do not consider any blockage corrections to our results.

Eleven different plate separations S were tested: 230, 240, 250, 260, 270, 280, 285, 290, 295, 300 and 305 mm. A right-handed coordinate system serves as reference, with $+x$ pointing downstream, $+y$ pointing to the bottom, and $+z$ pointing in spanwise direction. The origin is set at the centre point of the wind tunnel at the streamwise position of the plates. Thus, x marks the streamwise distance to the plane of the plates. Freestream velocity was kept constant at $U_\infty = 10$ m/s throughout the tests and was controlled and stabilised with a PID feedback system using the static pressure difference across the 9 : 1 wind tunnel contraction and the temperature inside the test-section measured half way along it. At that velocity, the fluctuations around the mean are below 0.1% when the test-section is empty. The resulting global Reynolds number for all datasets is $Re = U_\infty\sqrt{\mathcal{A}}/\nu = 4.3 \times 10^4$ (similar to values reported on previous experimental works on axisymmetric turbulent wakes [27–29]).

Hot-wire anemometry measurements were conducted downstream of the pair of plates using a Dantec Dynamics 55P01 single hot wire, driven by a Dantec StreamLine CTA system. The probe has a Pt-W wire, 5 μm in diameter, 3 mm long with a sensing length of 1.25 mm. The probe was placed with a levelling laser at the wind tunnel centre line and velocity profiles in streamwise direction were recorded with intervals of 10 mm. The probe can be located as close as 100 mm from the plates and up to 3020 mm away from them. For each probe location, the acquisition time was 60 s with a sampling frequency of 20 kHz. The traverse system is modular, allowing to automatize the acquisition of streamwise profiles over a 540 mm span. It can then be moved to cover different regions of the test section. Therefore, to measure sufficiently long streamwise distances, two or more profiles were recorded for each plate separation S. For the particular $S = 285$ mm case, a set of streamwise profiles covering the entire test section were performed for both kinds of plate. Therefore, for $S = 285$ mm, we have access to the whole streamwise evolution of the velocity temporal signal of the streamwise velocities.

To ensure continuity between individual streamwise profiles, the streamwise range covered by each one of them overlaps for approximately 100 mm with the next/previous profile. At the beginning of each single profile, a vertical wake profile was acquired between -250 mm$< y <$250 mm with $\Delta y = 20$ mm to verify U_∞ (acquisition time 30 s, frequency 20 kHz), and a new calibration of the hot wire was made to account for possible thermal drifts of the wind tunnel. Calibrations were made with a reference from a pitot tube located 50 mm below the hot-wire and for 9 equispaced velocities between 5 and 15 m/s. Temperature was monitored during the streamwise profiles, so it never

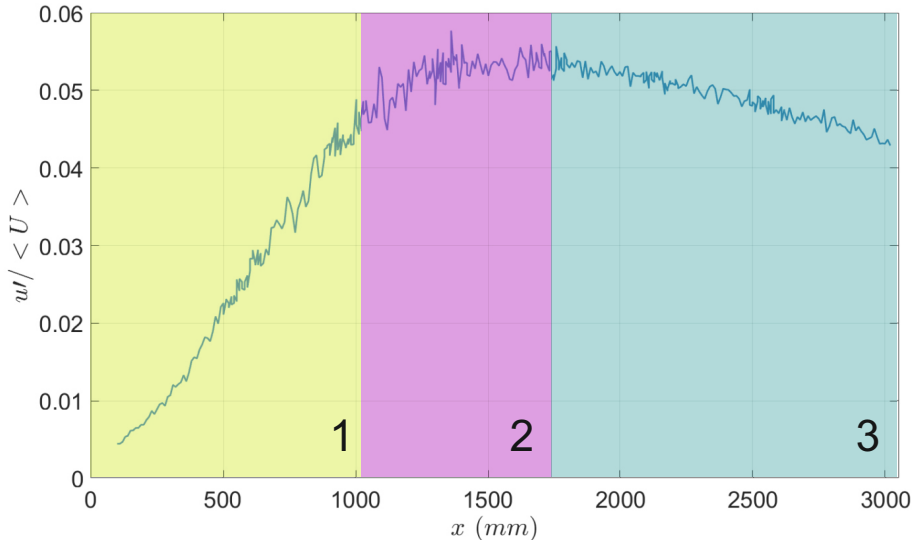

FIG. 2. Streamwise distribution of $u'/\langle U\rangle$ for the irregular plates at $S = 285mm$.

changed by more than 0.2°C.

The acquisition time of the centreline single wire measurements being 60 sec, an order of 1,000 integral time scales at each streamwise position were recorded thereby allowing good large-scale resolution. The Kolmogorov frequency was always smaller than half our sampling frequency (which is 20kHz) and the fluctuations are always below 10% (see figure 3a). We have also verified that, when the flow becomes turbulent ($x > 1$m), our sampling time corresponds to 3 to 10×10^3 integral time scales.

III. RESULTS - PLATES WITH IRREGULAR EDGES

A. Streamwise profiles and wake scale x_{12}

For a plate separation of 285 mm, streamwise velocity measurements along the entire test-section have been conducted. To capture this length, eleven single velocity profiles have been recorded. These measurements yield directly the local streamwise mean velocity $\langle U\rangle$ and the corresponding fluctuating velocity around this mean $u(t)$. Figure 2 shows the streamwise distribution of the velocity fluctuations $u'/\langle U\rangle$.

From figure 2 we identify three different regions in the flow (highlighted in the figure with different colours and labelled 1, 2 and 3). In region 1, both wakes have not met yet. It is important to remark that the boundaries of the wake are of statistical nature, and the flow can be affected by the generator at radial distances much higher than δ. This is the reason why the fluctuations show a monotonic increase in this region. Then, the profile of $u'/\langle U\rangle$ suggests that in region 2 the two wakes start to significantly interact and their boundaries meet more often than not, so that the velocity fluctuations reach a peak. This change of region is characterised by a sudden loss of linearity in the dependence of $u'/\langle U\rangle$ on x (present for example in the range $x \subset [500; 900]$ mm), as better detailed below. Further downstream, in region 3, both wakes are fully merged and the fluctuations exhibit a monotonic decrease.

For a better comprehension of the interactions regions, we study the properties of the flow at three representative streamwise locations: $x_1 = 500$ mm, $x_2 = 1500$ mm and $x_3 = 2500$ mm. Figures $3a, b$ &c show the time-signal of the streamwise fluctuating velocity $u(t)$ at these points. At x_1, the time signal of the fluctuating velocity is almost flat, with some extreme events. The spectrum is not turbulent yet (figure 3d), while the probability density function (PDF) of $u(t)$ (figure 3e) is far from Gaussian, and positively skewened. This behaviour is reminiscent of the findings in [30] for a turbulent grid flow, very close to the grid bars. Regions 2 and 3 show a better developed turbulent spectrum and a PDF which is still non-Gaussian, but has become negatively skewed. Figures 2 and 3 therefore suggest that the point x_{12} which demarcates between regions 1 and 2 might be related with the interaction of the two wakes and might be a good candidate for the wake interaction length x^*.

In the following, we test whether the wake width of the irregular plates scales according to the non-equilibrium dissipation law or not. To do so, we assume that the average edges of the two wakes meet where their wake extent $n\delta$ (with n close to 2) is equal to S. Figure 4 visualizes this configuration. Throughout this work, δ is always defined

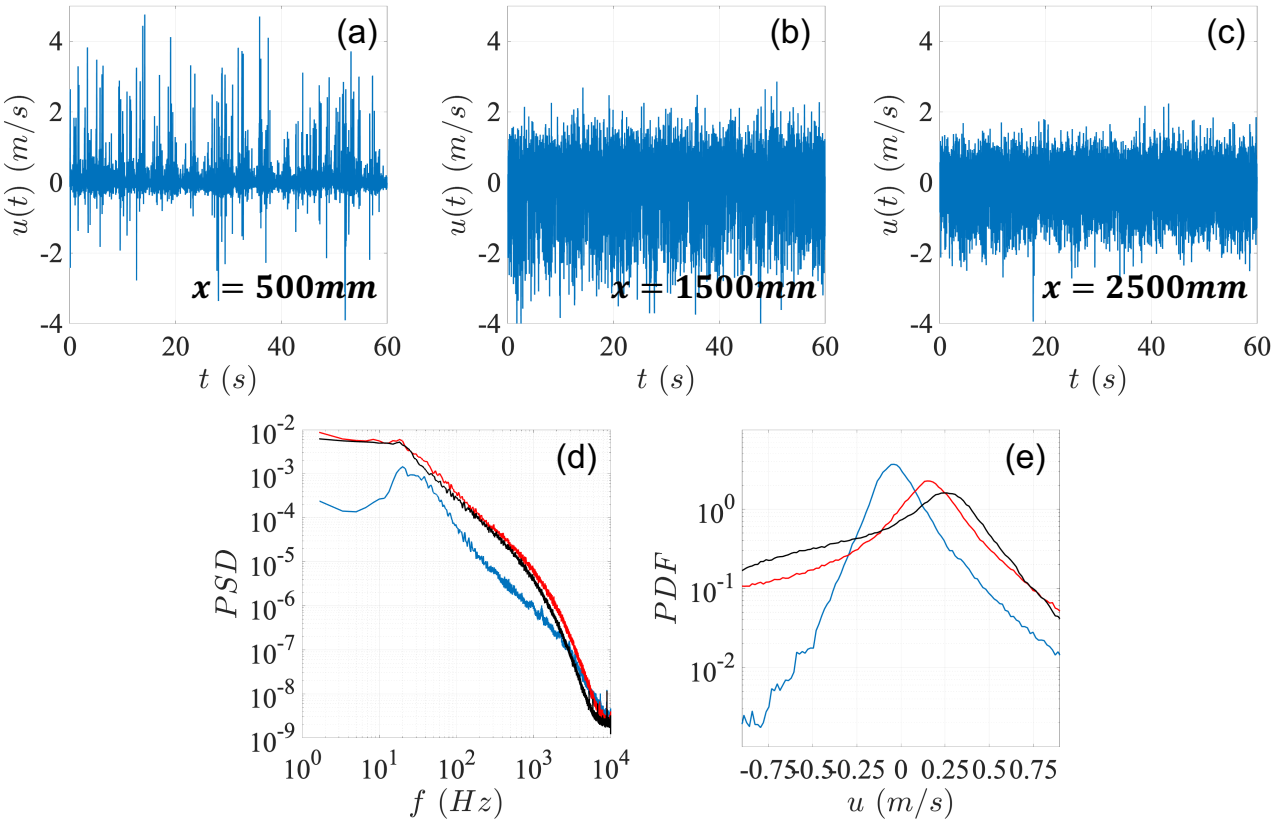

FIG. 3. Streamwise fluctuating velocity time signal $u(t)$ and its spectra and PDF at different locations for irregular plates at $S = 285$ mm. Time signal of $u(t)$ at $x_1 = 500$ mm (a), $x_2 = 1500$ mm (b) and $x_3 = 2500$ mm (c). Spectra at the three different locations (d), the blue line corresponds to x_1, the red one to x_2 and the black one to x_3. PDF of $u(t)$ (e) at the same locations and represented with the same colours as in (d). At x_1, the signal has a skewness of 3.0 and a flatness of 39.0. At x_2 they are -1.9 and 8.5, respectively. Finally, the signal at x_3 has a skewness of -1.1 and a flatness of 4.4.

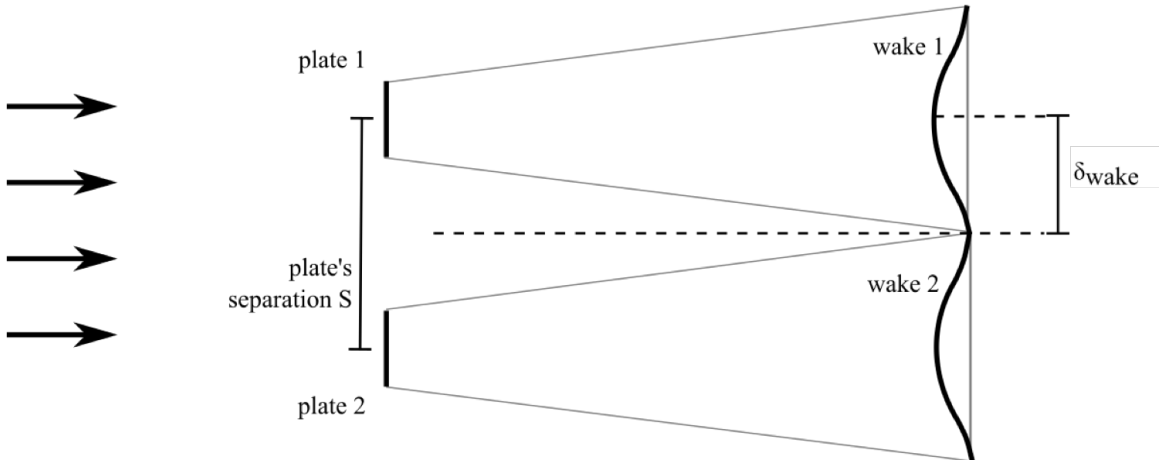

FIG. 4. Sketch of the interaction of both wakes when $0.5 \cdot S = n \cdot \delta$.

according to equation 4. In consequence, figure 4 only shows a schematised view of the interactions where it is assumed that the interaction will occur at $S \sim 2\delta$. Regarding this wake interaction process, we identify the location of the transition from region 1 to 2 (defined as x_{12}) as the beginning of significant interactions.

Figure 5b shows an example of the streamwise evolution of the normalised velocity fluctuations for the particular case $S = 270$mm (others are shown in figure 6a and present a similar shape). Regarding the wake interaction process, we interpret the transition point x_{12} from region 1 to 2 along the centreline streamwise axis to be the beginning

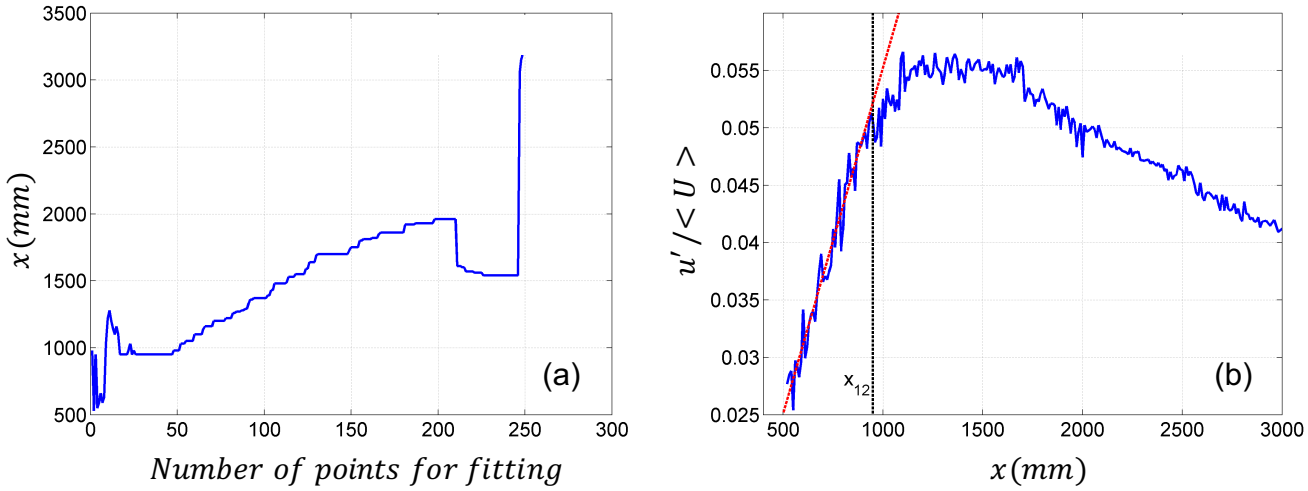

FIG. 5. Example illustrating the procedure of automatic detection of x_{12}. Location of minimum quadratic deviation as a function of the number of points used for the linear fit (a). x_{12} determined and its corresponding linear fit (b). Figures correspond to $S = 270mm$

of significant interactions between the two wakes in terms of turbulence velocity fluctuations. As we show in the present paper, the location x_{12} can be determined with simple hot-wire anemometry measurements in the streamwise direction only. The location x_{23} of the transition from regions 2 to 3 would require more complicated data collection and analysis methods (such as particle image velocimetry (PIV) and/or vertical hot-wire anemometry profiles) and we leave it for a further study.

It can be observed that region 1 is characterised by a linear relation between $u'/\langle U\rangle$ and x. We identify the streamwise transition point x_{12} as the point where this linearity is lost and use this property to determine x_{12} automatically for every case. To do so, the linear region is fitted locally for a given streamwise range, that is gradually increasing in number of points (i.e, for streamwise ranges that start on the smallest streamwise position and end on a distance that is increased between subsequent fits). Plotting the location x_{min} of lowest quadratic deviation versus the number of points used for the linear interpolation, the location x_{12} can be detected by the first plateau region within this plot (other plateaux may exist for larger x_{min} due to the change of concavity that occurs within region 2). An example of this procedure is shown in figures 5a& b.

The streamwise locations found by this automatic procedure are represented by the black squares in figure 6a. A summary of the locations x_{12} identified by this process is given in table I. To determine the factor n, we use the scaling law of the wake half width of a single wake:

$$\frac{\delta(x)}{\theta} = B\left(\frac{x - x_0}{\theta}\right)^{\beta}, \tag{7}$$

where $\delta(x)$ is the wake-width at position x, θ is momentum thickness of the plate, x_0 stands for a virtual origin of the plate, and B and β are fitting parameters. For the irregular plates used herein, [13] found the following values in agreement with the non-equilibrium dissipation law: $\theta = 21\,\mathrm{mm}$, $x_0/\theta = -5.35$, $B = 0.37$, and $\beta = 0.52$. We remark that these values were obtained experimentally in the same wind tunnel, using the same equipment and plates, and therefore remain valid for the modeling of the single wake evolution of the plates studied here. Using these values and equation 7, we can set up equation 8,

$$\frac{1}{n}\cdot\frac{S}{2\,\theta} = B\left(\frac{x_{12} - x_0}{\theta}\right)^{\beta}, \tag{8}$$

and solve it for n for every plate separation tested. The values thus obtained for n are given in table I.
Perhaps remarkably, all n-factors are found to be close to the mean value $\langle n\rangle = 2.26$. This result indicates that significant wake interactions take place where $2.26 \cdot \delta(x)$ is equal to the plate separation.

This result supports the validity of the non-equilibrium dissipation law in the wake of the irregular plates and determines the beginning of wake interactions on the basis of the non-equilibrium scalings of the wake half width.

TABLE I. Overview of transition locations between region 1 & 2 obtained for irregular plates

S [mm]	230	240	250	260	270	280	285	290	295	300	305
x_{12} [mm]	670	710	790	890	950	1030	1040	1110	1150	1190	1230
n	2.26	2.29	2.28	2.24	2.26	2.26	2.29	2.26	2.26	2.26	2.26
$\langle n \rangle$	2.26										
$\sigma_n/\langle n \rangle$	0.0068										

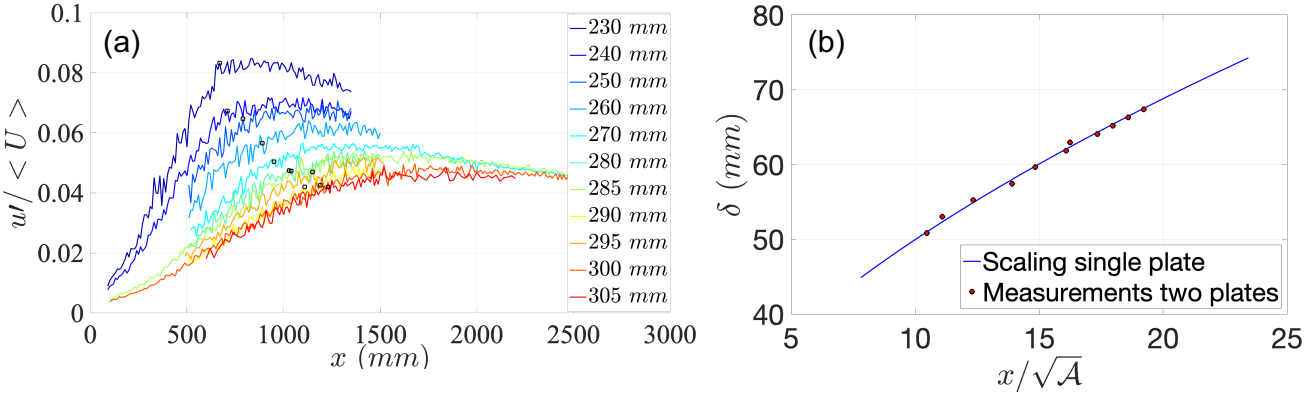

FIG. 6. (a) Streamwise profile of the velocity fluctuations for all plate separations S in table I. The black squares represent x_{12}, i.e. the x-locations of the transition between regions 1 and 2; (b) Comparison of the wake half width profile obtained for a single irregular plate by [13] (blue line) with the results obtained using equation 9 in the wake-interaction setup used here (red circles).

Combining equations 7 & 8, a single wake half width δ_{wake} can be defined from the interaction between two plates,

$$\delta_{wake}(x_{12}) = S/(2\,\langle n \rangle), \tag{9}$$

where for each plate separation S, one value of δ_{wake} can be estimated using its corresponding value of x_{12} and the averaged value $\langle n \rangle$. We remark that, in equation 9, the averaged value $\langle n \rangle$ depends on the set of parameters B, x_0 and β, and therefore carries infirmation about the energy cascade within the wakes. To underscore this result, figure 6b shows the streamwise evolution of the wake half width with increasing streamwise position from the plate as obtained for a single plate by [13] (blue line) and compared to δ_{wake} (red dots). Again, the results coincide. It is therefore possible to predict the overall level of the streamwise profile of $\delta(x)$, which is a characteristic of the mean flow cross-stream profile of a single wake, by acquiring velocity fluctuation measurements in regions 1 and 2 of a two-wake set-up.

We finish this section by assessing the consistency of x_{12} as the onset of interaction between wakes and the possibility of using other parameters to quantify this phenomenon. For instance, figure 3a suggest that the intermittency of $u(t)$ could also be used as a criterion to set the value of x_{12}. We define an intermittency factor via an intermittency function I(t), that is defined as one for a turbulent flow and as 0 for a non-turbulent one [31, 32]. Given that we look to quantify the large-scale intermittency of $u(t)$, we can define this function using a threshold u^2_{th} for the time-signal of $u(t)^2$,

$$\mathrm{I} = \begin{cases} 1\ if\ u(t)^2 > u^2_{th} \\ 0\ if\ u(t)^2 \leq u^2_{th} \end{cases} \tag{10}$$

Then, the intermittency factor γ is defined as,

$$\gamma = \langle \mathrm{I} \rangle = \frac{1}{T_s} \int_{t=0}^{T_s} \mathrm{I}(t) dt \tag{11}$$

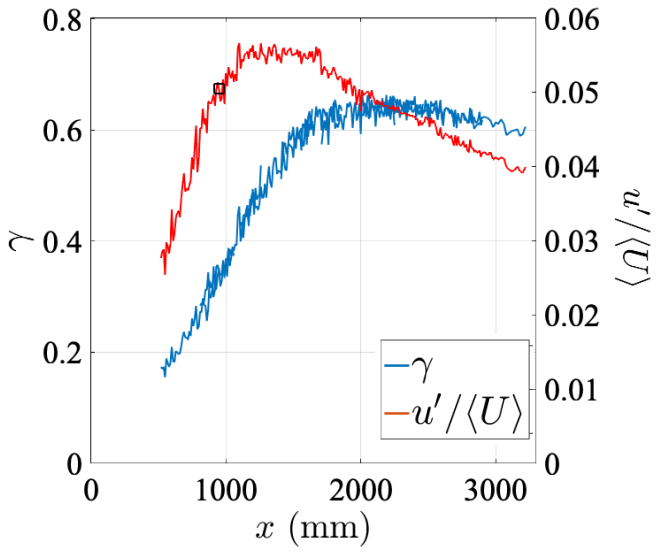

FIG. 7. Streamwise evolution of the intermittency factor γ obtained using equations 10 & 11 (blue line), and compared to the turbulence intensity ($u'/\langle U \rangle$, red line). The threshold used is $u_{th}^2 = 0.05$ m^2/s^2, while other values give identical trends with different absolute values. The curves were obtained for a pair of irregular plates with a separation $S = 270$ mm.

for a long enough integration time T_s.

Figure 7 shows the streamwise evolution of γ compared to the turbulence intensity for a separation between plates of $S = 270$ mm. For this particular separation it was found (table I) that $x_{12} = 950$ mm. While γ does show a change of behaviour that could be used to quantify the interaction between two plates, figure 7a hints that it may be rather related to x_{23}. As stated above, future works using 2D and 3D visualisation of the velocity field could help to understand the role of γ in the transition between the second and the third regimes.

B. Higher-Order Moments

In previous studies, wake interactions have been investigated in terms of higher-order moments, such as velocity skewness and flatness [20, 30]. Figure 8a and 8b show the skewness and flatness profiles for all plate separations tested. The behavior of both moments is quite similar to the results of [20, 30]. These two studies investigated 2D planar wakes of bars of turbulence-generating grids. In contrast, the wakes in the current study are 3D and axisymmetric. Hence, figure 8a provides experimental evidence that high-order moments can evolve similarly in the streamwise direction in 2D planar and 3D axisymmetric wakes. The detailed analysis of this finding is left for future studies.

A previous study [20] showed that the skewness and flatness profiles of different turbulence grids could be collapsed by scaling the streamwise position with a wake-interaction length scale x_*. Subsequently, [21] collapsed velocity fluctuation profiles of different experiments with an improved wake-interaction length scale x'_*. In figures 9a and 9b the skewness and flatness profiles are replotted with the x-axis scaled by the length-scale x_{12} discussed earlier. We find that all values of S collapse (we note that the figure is in linear scales), with the exception of the smallest separation; $S = 230mm$. The reason for this exception may be that the wakes meet before having become self-similar or axisymmetric for this low value of S. Moreover, for small values of S different phenomena can arise in the interaction of near wakes. For instance, for square bars three different regimes can be identified depending on the ratio between the bars' separation and their size [33]. To the authors' best knowledge, no similar study has been performed for bluff plates, and further research could clarify this point.

In the following sub-section, we further test the idea that the length-scale x_{12} is a wake-interaction length-scale and show also that it can be used to scale the streamwise profile of the turbulent velocity fluctuations.

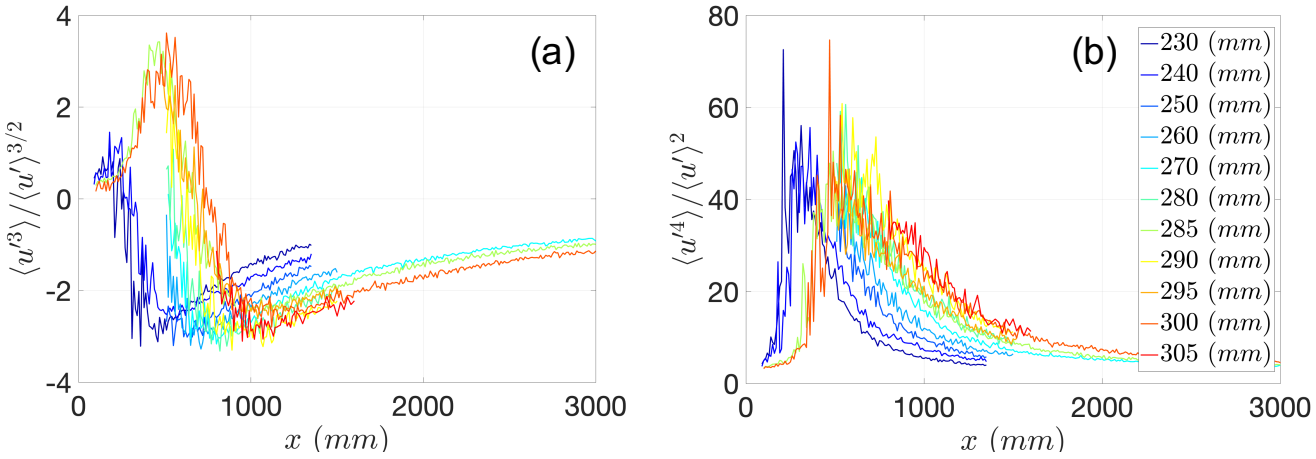

FIG. 8. (a) Skewness and (b) flatness profiles for all plate separations tested. The separation increases from left to right.

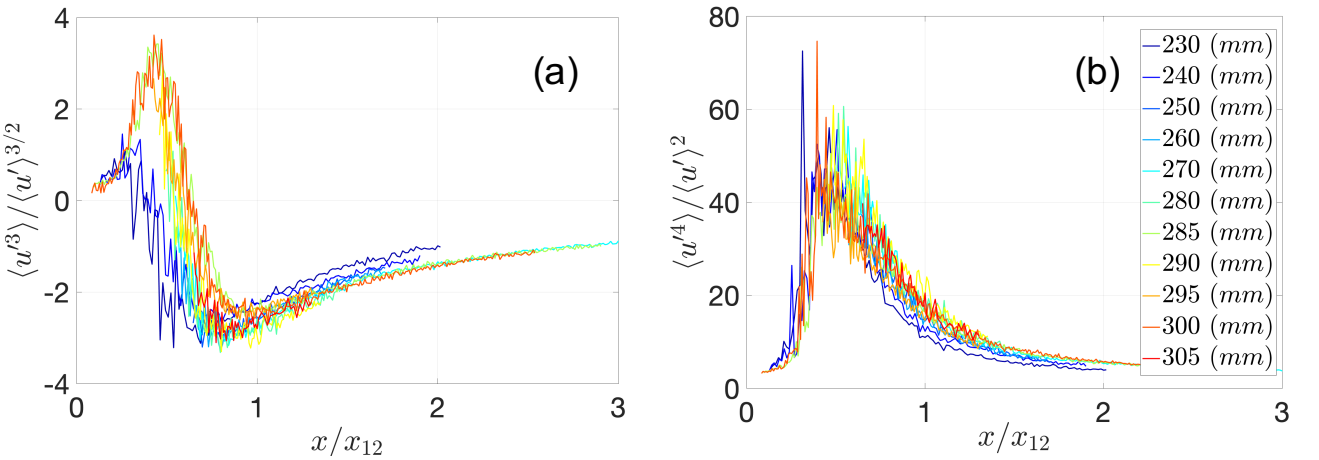

FIG. 9. (a) Skewness and (b) flatness profiles for all plate separations tested. The streamwise position x is scaled by the length-scale x_{12}.

C. Wake-Interaction Length Scale

As stated above, [20] and [21] proposed formulae for a wake-interaction length scale characterising the interaction of planar wakes emanating from fractal and regular grids. This length-scale can be easily constructed for any free-shear flow. In our case, two axisymmetric wakes can be surely expected to interact at a streamwise distance x^* from the plates where δ (defined via equation 4) is expected to be close to half the distance between the centres of the plates (defined as S in this work). This implies that the wake interaction length x^* scales as $x^* \propto S^2$ on the basis of equation 6, resulting in

$$\left(\frac{x^* - x_0}{\theta}\right) \propto \left(\frac{S}{2\theta}\right)^2. \tag{12}$$

A crucial step in the wake interaction approach of [21] is the neglect of the virtual origin x_0 because the *"distance downstream where the wakes meet is very much larger than the virtual origin. We therefore ignore the virtual origin x_0 and effectively set it equal to zero."* In our case, this would imply that $x^* \gg x_0$, which we find below to hold for all cases (see table II).

We can then define a modified wake interaction length for two axisymmetric plates in the non-equilibrium regime by,

TABLE II. Wake-interaction length scale values obtained for irregular plates

S [mm]	230	240	250	260	270	280	285	290	295	300	305
x_{12} [mm]	670	710	790	890	950	1030	1040	1110	1150	1190	1230
x'_* [mm]	630	686	744	805	868	933	967	1001	1036	1071	1107
x'_*/x_{12}	0.94	0.97	0.94	0.90	0.91	0.91	0.93	0.90	0.90	0.90	0.90

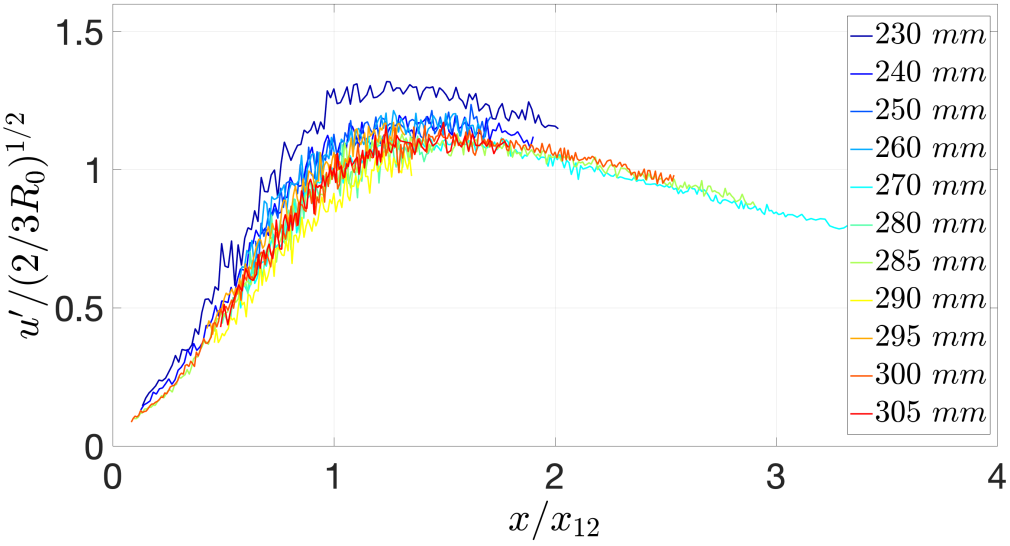

FIG. 10. Profiles of u' obtained for plates with irregular peripheries normalised according to according to $u' \sim \sqrt{2/3R_0}F(x/x_{12})$, where $R_0 = U_\infty u_0(d/dx\,\delta(x))$.

$$x'_* = \phi\frac{S^2}{4\theta}. \tag{13}$$

where ϕ is a constant that depends on the geometry of the plates and accounts for the contributions of B and $\langle n\rangle$.

The wake-interaction length scale x'_* based on equation 13 is given in table II for different values of S together with the length scale x_{12} determined earlier. It can be seen that x_{12} and x'_* are proportional to each other (and in fact do not differ by more than 10%). Hence, the length scale x_{12}, determined empirically, scales with the modified wake-interaction length scale x'_* based on the non-equilibrium dissipation law. It is therefore possible to consider x_{12} as the wake interaction length for turbulent axisymmetric wakes. As a result, the length scale x_{12} can be used to collapse the streamwise development of the turbulence intensities. To complete the scaling of the turbulence intensity we note that, in the case of a single wake, the turbulent kinetic energy and the Reynolds shear stress evolve together in the streamwise direction [13–15] and that the Reynolds shear stress scales with streamwise distance as $U_\infty u_0(d/dx\,\delta(x))$ (see [13, 15]). We therefore attempt the scaling $u' \sim \sqrt{U_\infty u_0(d/dx\,\delta(x))}F(x/x_{12})$ where F is a dimensionless function of x/x_{12}. In this work we did not measure the values of $u_0(x)$ and $\delta(x)$ and we therefore used their fits from [13] for the irregular plates.

In figure 10 we show the velocity fluctuations normalised according to $u' \sim \sqrt{U_\infty u_0(d/dx\,\delta(x))}F(x/x_{12})$. Most of the profiles collapse fairly well. Consistently with the discussion in sub-section 3.2, the collapse is worse for smaller values of S.

IV. RESULTS - REGULAR SQUARE PLATES

As discussed above, in addition to the two plates with irregular peripheries, two regular square plates with the same area ($\sqrt{\mathcal{A}} = 64$ mm) were also investigated. Again eleven different separations were set and the same measurements

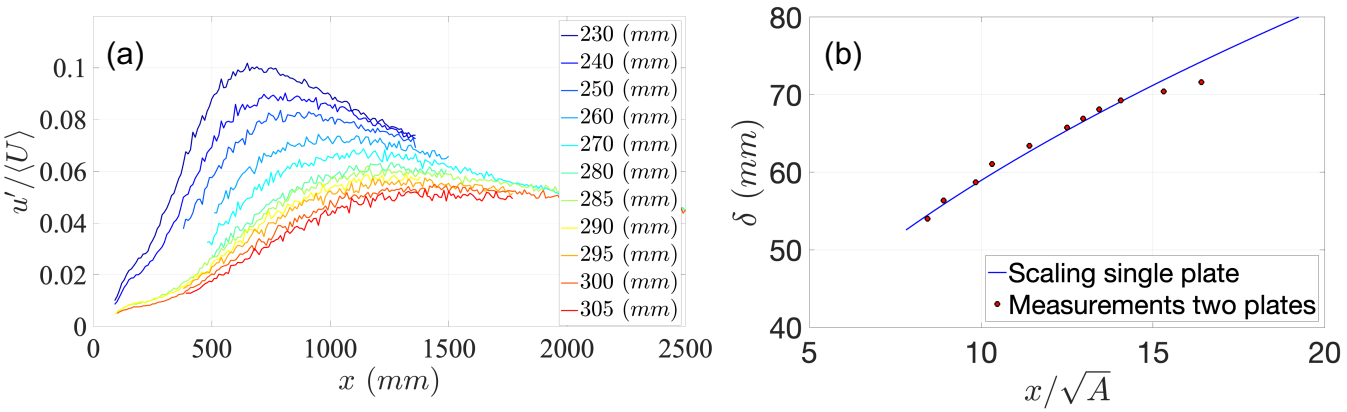

FIG. 11. (a) Streamwise distribution of the velocity fluctuations for all square plate's separations given in table I. (b) Comparison of the wake-width distribution found for a single regular plate by [6] (blue line) and the results gained using equation 9 in the wake-interaction setup used herein (red circles). The parameters of equation 7 corresponding to square plates are $\theta = 19.7\,\text{mm}$, $x_0/\theta = -6.20$, $B = 0.494$, and $\beta = 0.50$ [6].

TABLE III. Overview of the length-scale x_{12} and other parameters chacraterizing the wake's interaction for the square plates

S [mm]	230	240	250	260	270	280	285	290	295	300	305
x_{12} [mm]	540	570	630	660	730	800	830	860	900	980	1050
n	2.11	2.15	2.14	2.17	2.15	2.14	2.14	2.14	2.14	2.09	2.05
$\langle n \rangle$	2.13										
$\sigma_n/\langle n \rangle$	0.016										
x'_* [mm]	671	731	793	858	925	995	1031	1067	1104	1142	1181
x'_*/x_{12}	1.24	1.28	1.26	1.30	1.27	1.24	1.24	1.24	1.23	1.17	1.12

as for the irregular plates were conducted. Figure 11a shows the streamwise development of the velocity fluctuations for all separations. The shapes of these profiles are similar to those for the irregular plates.

Again, we determine the length-scale x_{12} at the point of transition from region 1 to 2 in the turbulent fluctuations streamwise profile (see figure 11a). The results of this automated procedure are given in table III. The n-factor is once again very similar for all values of S, but slightly different from the irregular plates: $\langle n \rangle = 2.13$. Figure 11b compares the wake-width based on the identified length-scale x_{12} with the results of the single-plate measurements of [6]. Equation 13 yields the modified wake-interaction length scale x'_* for these regular square plates (see table III). As found for the irregular plates, our length-scale x_{12} is a multiple of x'_*, in this regular case with $x_{12} = 1.24 \cdot x'_*$.

To evaluate the collapse capability of x_{12}, we scale the streamwise profile of the higher-order moments (skewness and flatness) of the velocity fluctuations with x_{12}. In figures 12a and 12b we plot the original skewness and flatness profiles and in figures 12c and 12d we plot the streamwise skewness and flatness profiles scaled with x_{12}. Some collapse, particularly for the larger values of S is, once again, observed.

Finally, in figure 13, x_{12} is used to collapse the streamwise profile of velocity fluctuations. Streamwise velocity fluctuations are scaled according to $u' \sim \sqrt{U_\infty u_0 (d/dx\, \delta(x))} F(x/x_{12})$ as for the irregular plates. A fairly good collapse of the profiles is obtained again except for the smaller values of S.

V. RESULTS - COMPARISON BETWEEN IRREGULAR AND REGULAR PLATES

In this section we proceed to compare results obtained for both sets of plates. For instance, it can be observed that, while collapse is acceptable for all cases, it may differ between types of plates. Indeed, irregular plates have been found to require a longer streamwise distance to become self similar [34]. They also have, for a fixed streamwise position, smaller values of δ. This implies that for different types of plates, a given separation S may differed when expressed as multiples of δ.

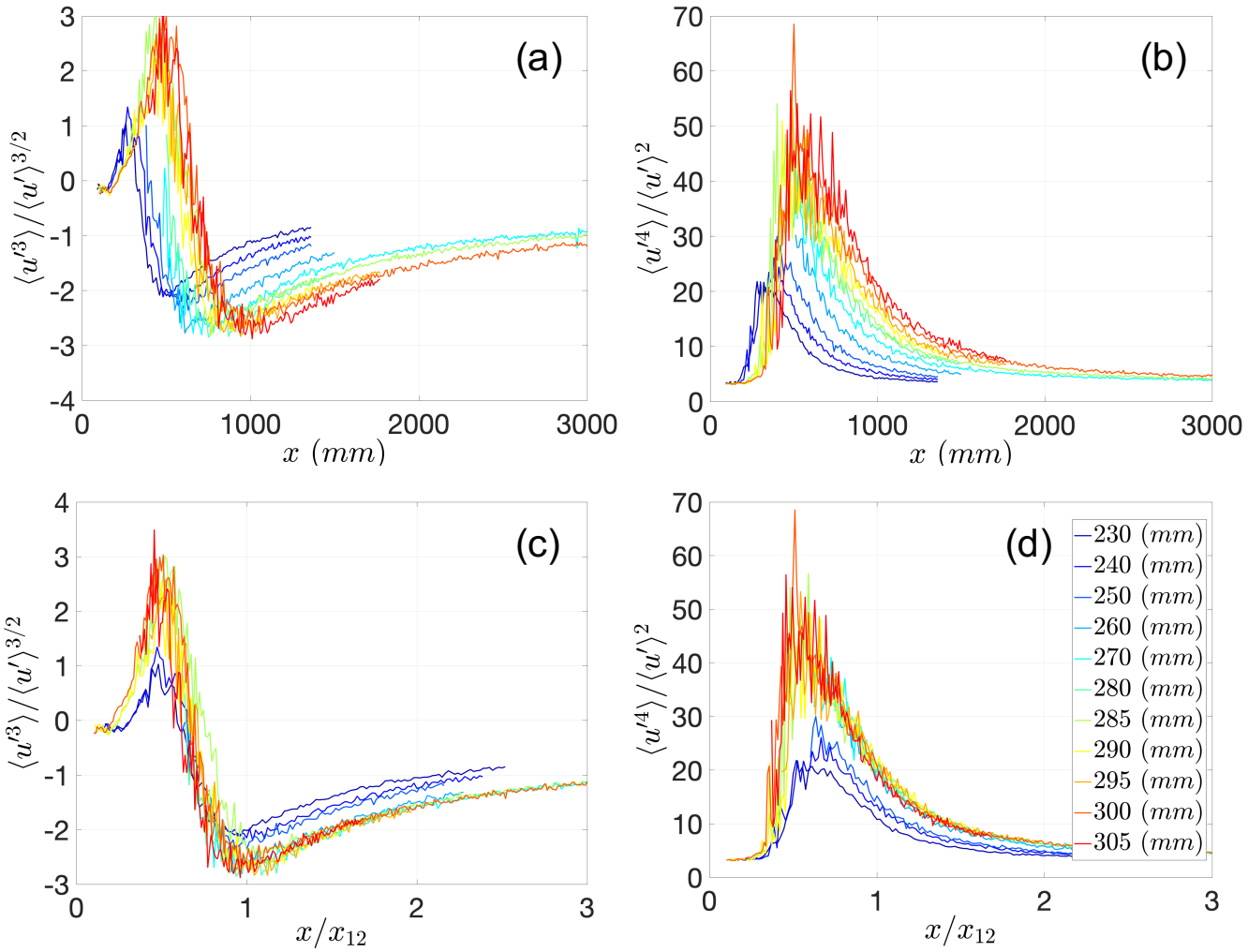

FIG. 12. (a, b) Unscaled skewness and flatness profiles for all square plate separations tested. (c, d) Skewness and flatness profiles scaled with x_{12}.

We therefore proceed to compare the major results from the irregular and the regular square plates. We focus on $S \geq 260$mm, where the profile collapse is best in terms of x_{12}. In figure 14a and 14b we plot the streamwise profiles of the skewness and the flatness of the turbulent velocity fluctuations scaled by the interaction length scale x_{12} for both the irregular and the regular set of square plates. A reasonable collapse is achieved. In figure 15, the streamwise profiles of the scaled velocity fluctuations are displayed. It can be seen that the maxima of $u'/\sqrt{(2/3R_0)}$ (where $R_0 = U_\infty u_0(d/dx\,\delta(x))$) are higher for the regular plates than for the irregular ones. The scaling $u' \sim \sqrt{U_\infty u_0(d/dx\,\delta(x))}F(x/x_{12})$ seems to hold for both sets of plates, but the proportionality constant is different depending on plate geometry. Further studies covering geometries not covered in this work could help to better understand the dependency of the function $F(x/x_{12})$ with different parameters such as the plate's edges, drag coefficient, etc...

VI. CONCLUSIONS

In this work we have studied experimentally via hot-wire anemometry the interaction between two turbulent axisymmetric wakes in the wind tunnel. The wake generators were pairs of plates, one pair with plates of regular peripheries and one pair with plates of irregular peripheries. We first pointed out that the wake interaction length x^* can be quantified using only streamwise profiles of the turbulence intensity in the symmetry axis between both plates. Furthermore, we find that x^* is related to the wake half width $\delta(x)$ and the separation between plates S

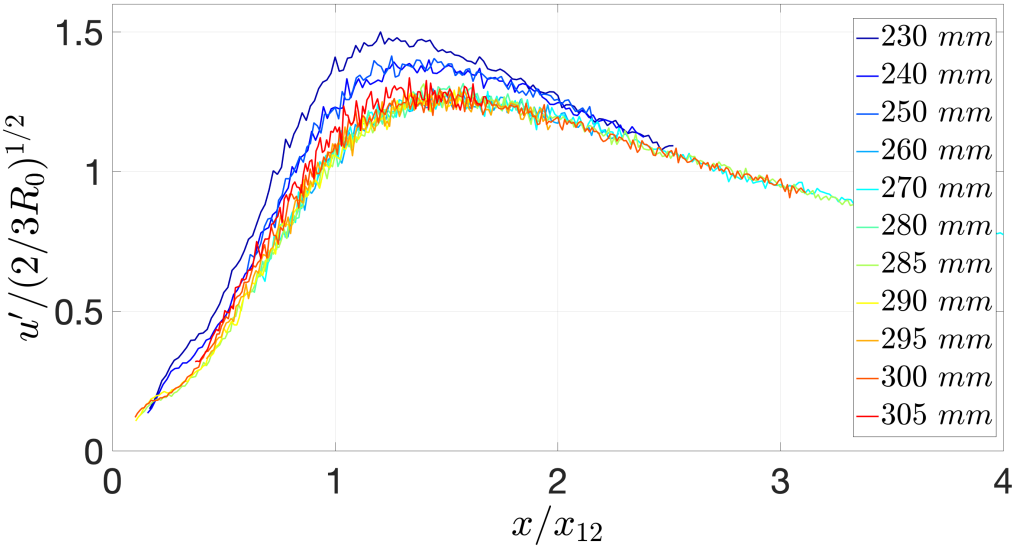

FIG. 13. Profiles of u' obtained for plates with square peripheries normalised according to equation $u' \sim \sqrt{2/3R_0}F(x/x_{12})$ where $R_0 = U_\infty u_0(d/dx\,\delta(x))$.

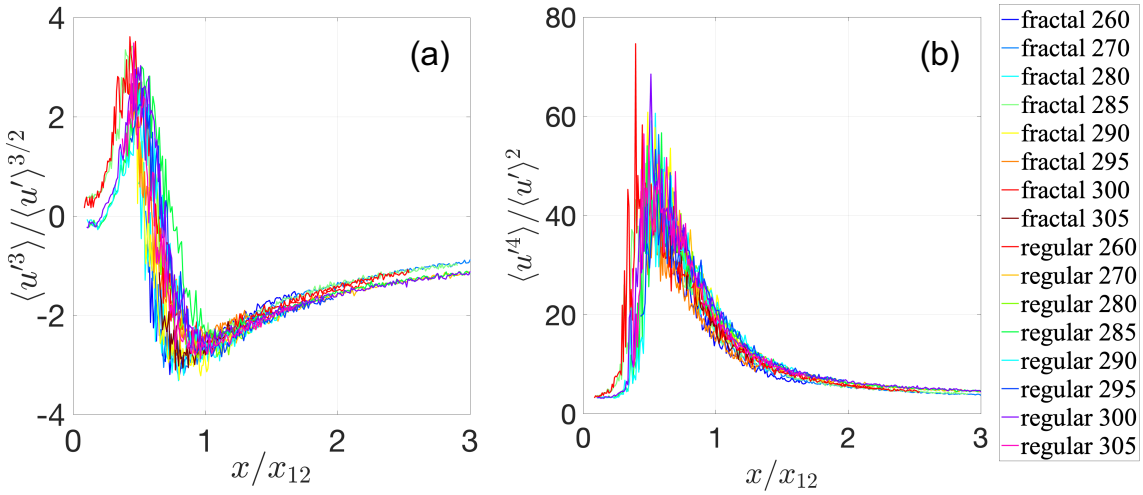

FIG. 14. Scaled skewness and flatness of irregular and regular plates

as $S \approx 2.26\delta(x^*)$. By acquiring streamwise profiles for different plate separations and identifying the wake interaction length for each separation it is possible to show that the interaction between the wakes is consistent with non-equilibrium scalings. The profile of the streamwise distribution of the normalised velocity fluctuations $u'/\langle U\rangle$ is used to characterise the interaction of two wakes, as it shows three clearly defined regions: a first region where the wakes have not significantly met yet and the flow is highly intermittent and a second region where the wakes start to merge and where $u'/\langle U\rangle$ reaches a maximum value. Finally, in the third region both wakes are fully merged and the fluctuations exhibit a monotonic decrease with streamwise distance.

We have therefore proposed to identify the wake interaction length with the streamwise point x_{12} where the flow goes from region 1 to region 2. We find that the values of x_{12} are indeed consistent with the non-equilibrium cascade, as $x_{12} \propto S^2$. Indeed, as explained in the introduction, for the case of the standard Richardson-Kolmogorov energy cascade, x^* evolves as S^3, while a non-equilibrium cascade implies $x^* \propto S^2$.

We also defined a wake interaction length-scale independently from x_{12} and have shown that it is proportional to x_{12}. We then used x_{12} to successfully collapse the streamwise profiles of the second, third and fourth moments of the streamwise fluctuating velocity.

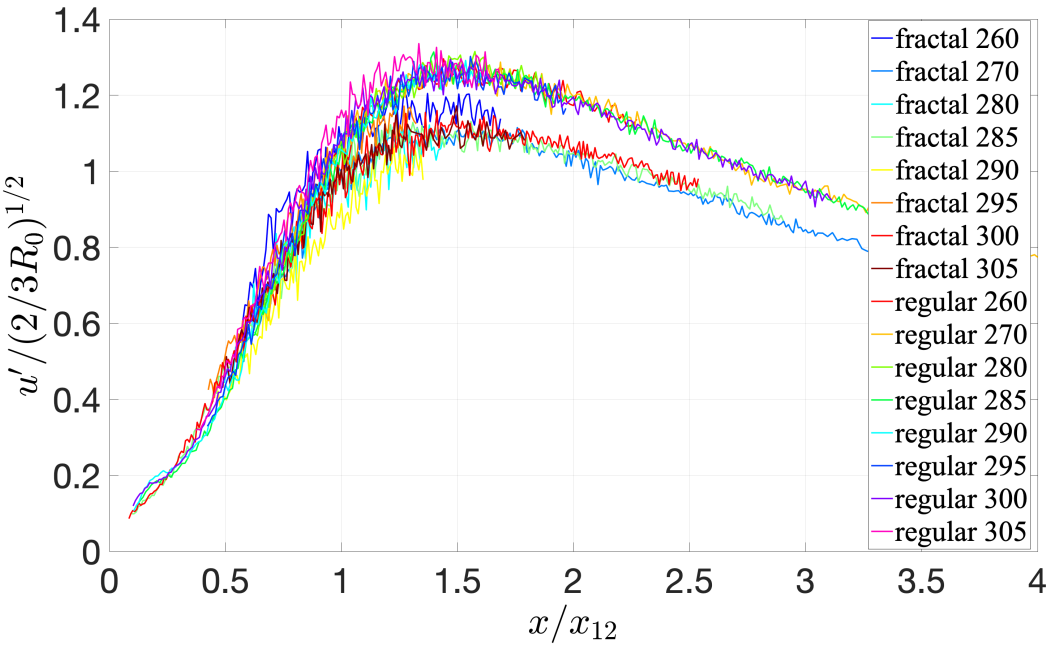

FIG. 15. Scaled u' of the irregular and regular square plates.

Following previous theoretical developments [13–15] which demonstrated that the turbulent kinetic energy and the Reynolds shear stress both scale with streamwise distance as $U_\infty u_0(d/dx\,\delta(x))$ we have proposed the scaling $u' \sim \sqrt{U_\infty u_0(d/dx\,\delta(x))}F(x/x_{12})$ where F is a dimensionless function of x/x_{12}. This scaling holds for both sets of plates, but the proportionality constant is larger for the regular than the irregular plates.

Our results and analysis could contribute to the study of interactions between wakes of neighboring wind turbines and the design of wind farms. Further experimental studies using PIV or direct numerical simulations can help to give further ingsight into the properties of the wake across the three regions we have identified in this work.

ACKNOWLEDGMENTS

We acknowledge the support of ERC Advanced Grant 320560 awarded to JCV.

[1] J. Vassilicos, Dissipation in turbulent flows, Ann. Rev. Fluid Mech. **47**, 10.1146/annurev-fluid-010814-014637 (2015), http://dx.doi.org/10.1146/annurev-fluid-010814-014637.
[2] K. Chongsiripinyo and S. Sarkar, Decay of turbulent wakes behind a disk in homogeneous and stratified fluids, Journal of Fluid Mechanics **885** (2020).
[3] K. Takamure, Y. Sakai, Y. Ito, K. Iwano, and T. Hayase, Dissipation scaling in the transition region of turbulent mixing layer, International Journal of Heat and Fluid Flow **75**, 77 (2019).
[4] D. C. Saunders, J. A. Britt, and S. Wunsch, Decay of the drag wake of a sphere at reynolds number 10^5, Experiments in Fluids **63**, 1 (2022).
[5] J. Nedić, J. Vassilicos, and B. Ganapathisubramani, Axisymmetric turbulent wakes with new nonequilibrium similarity scalings, Physical review letters **111**, 144503 (2013).
[6] M. Obligado, T. Dairay, and J. C. Vassilicos, Nonequilibrium scalings of turbulent wakes, Physical Review Fluids **1**, 044409 (2016).
[7] Y. Zhou and J. Vassilicos, Related self-similar statistics of the turbulent/non-turbulent interface and the turbulence dissipation, Journal of Fluid Mechanics **821**, 440 (2017).
[8] M. van Reeuwijk, J. C. Vassilicos, and J. Craske, Unified description of turbulent entrainment, Journal of Fluid Mechanics **908**, A12 (2021).

[9] G. Cafiero and J. Vassilicos, Non-equilibrium turbulence scalings and self-similarity in turbulent planar jets, Proceedings of the Royal Society A **475**, 20190038 (2019).

[10] G. Cafiero and J. C. Vassilicos, Non-equilibrium scaling of the turbulent-nonturbulent interface speed in planar jets, Physical Review Letters **125**, 174501 (2020).

[11] M. Breda and O. R. Buxton, Influence of coherent structures on the evolution of an axisymmetric turbulent jet, Physics of Fluids **30**, 035109 (2018).

[12] G. Cafiero, M. Obligado, and J. C. Vassilicos, Length scales in turbulent free shear flows, Journal of Turbulence **21**, 243 (2020).

[13] T. Dairay, M. Obligado, and J. Vassilicos, Non-equilibrium scaling laws in axisymmetric turbulent wakes, Journal of Fluid Mechanics **781**, 166 (2015).

[14] A. Townsend, *The structure of turbulent shear flow* (Cambridge university press, 1976).

[15] W. George, The self-preservation of turbulent flows and its relation to initial conditions and coherent structures, Advances in Turbulence , 39 (1989).

[16] I. Neunaber, M. Hölling, R. J. Stevens, G. Schepers, and J. Peinke, Distinct turbulent regions in the wake of a wind turbine and their inflow-dependent locations: the creation of a wake map, Energies **13**, 5392 (2020).

[17] I. Neunaber, J. Peinke, and M. Obligado, Investigation of the dissipation in the wake of a wind turbine array, Wind Energy Science Discussions , 1 (2021).

[18] R. Scott, B. Viggiano, T. Dib, N. Ali, M. Hölling, J. Peinke, and R. B. Cal, Wind turbine partial wake merging description and quantification, Wind Energy **23**, 1610 (2020).

[19] J. Ortiz-Tarin, S. Nidhan, and S. Sarkar, High-reynolds-number wake of a slender body, Journal of Fluid Mechanics **918** (2021).

[20] N. Mazellier and J. Vassilicos, Turbulence without richardson–kolmogorov cascade, Physics of Fluids (1994-present) **22**, 075101 (2010).

[21] R. Gomes-Fernandes, B. Ganapathisubramani, and J. Vassilicos, Particle image velocimetry study of fractal-generated turbulence, Journal of Fluid Mechanics **711**, 306 (2012).

[22] H. Zong and F. Porté-Agel, A momentum-conserving wake superposition method for wind farm power prediction, Journal of Fluid Mechanics **889** (2020).

[23] M. Bastankhah, B. L. Welch, L. A. Martínez-Tossas, J. King, and P. Fleming, Analytical solution for the cumulative wake of wind turbines in wind farms, Journal of Fluid Mechanics **911** (2021).

[24] I. Neunaber, M. Obligado, J. Peinke, and S. Aubrun, Application of the townsend-george wake theory to field measurements of wind turbine wakes, in *Journal of Physics: Conference Series*, Vol. 1934 (IOP Publishing, 2021) p. 012004.

[25] M. F. van Dooren, A. P. Kidambi Sekar, L. Neuhaus, T. Mikkelsen, M. Hölling, and M. Kühn, Modelling the spectral shape of continuous-wave lidar measurements in a turbulent wind tunnel, Atmospheric Measurement Techniques **15**, 1355 (2022).

[26] J. Nedić, B. Ganapathisubramani, and J. Vassilicos, Drag and near wake characteristics of flat plates normal to the flow with fractal edge geometries, Fluid Dynamics Research **45**, 061406 (2013).

[27] P. B. V. Johansson, W. K. George, and M. J. Gourlay, Equilibrium similarity, effects of initial conditions and local reynolds number on the axisymmetric wake, Physics of Fluids **15**, 603 (2003).

[28] O. Ilday, H. Acar, M. K. Elbay, and V. Atli, Wakes of three axisymmetric bodies at zero angle of attack, AIAA journal **31**, 1152 (1993).

[29] A. Taylor and J. Whitelaw, Velocity characteristics in the turbulent near wakes of confined axisymmetric bluff bodies, Journal of fluid mechanics **139**, 391 (1984).

[30] S. Laizet, J. Nedić, and J. C. Vassilicos, The spatial origin of- 5/3 spectra in grid-generated turbulence, Physics of Fluids (1994-present) **27**, 065115 (2015).

[31] S. Pope, *Turbulent flows* (Cambridge university press, 2000).

[32] L. S. Kovasznay, V. Kibens, and R. F. Blackwelder, Large-scale motion in the intermittent region of a turbulent boundary layer, Journal of Fluid Mechanics **41**, 283 (1970).

[33] J. Chen, C. Cuvier, J.-M. Foucaut, Y. Ostovan, and J. Vassilicos, A turbulence dissipation inhomogeneity scaling in the wake of two side-by-side square prisms, Journal of Fluid Mechanics **924** (2021).

[34] J. Nedic, *Fractal-generated wakes*, Ph.D. thesis, Imperial College London (2013).